Nanotexture influence of $BaTiO_3$ particles on piezoelectric behaviour of PA 11/$BaTiO_3$ nanocomposites

Jean-Fabien Capsal [a], Eric Dantras [a,*], Lydia Laffont [b], Jany Dandurand [a], Colette Lacabanne [a]

[a] Laboratoire de Physique des Polymères, Institut CARNOT – CIRIMAT, Université Paul Sabatier, 31062 Toulouse, France
[b] ENSIACET, MEMO, Institut CARNOT – CIRIMAT, Toulouse, France

A B S T R A C T

The piezoelectric activity of a hybrid ferroelectric nanocomposite, i.e. polyamide 11/barium titanate (BT), has been investigated for different loadings of BT particles. The BT volume fraction (ϕ) was ranging from 0.024 to 0.4 with a particle size of 50, 100, 300 and 700 nm. The influence of polarization mode on the piezoelectric behaviour has been studied. The magnitude of the poling field used in this study is in the same order of magnitude of the one used for bulk BT i.e. significantly lower than for piezoelectric polymers. The optimum piezoelectric coefficient is reached when the amorphous phase of the polymeric matrix is in the liquid state i.e. for a polarization temperature higher than the glass transition and for time constant allowing macromolecular mobility. The composite piezoelectric activity decreases for particles size lower than 300 nm due to the loss of the tetragonal phase. The nanotexture of these particles has been investigated by transmission electron microscopy (TEM) and high-resolution TEM. A core shell structure has been observed. An increase of the longitudinal piezoelectric strain coefficient d_{33} with the raising of BT volume fraction was shown. Contrary to inorganic piezoelectric ceramics, the dielectric permittivity of hybrid composites remains moderate; therefore it allows the piezoelectric voltage coefficient of composites to be higher than ceramics.

Keywords:
Dielectric properties
Relaxation
Electric modulus
Piezoelectric
STEM/TEM
Nanocomposites
Nanoparticles
Polymers and organics

1. Introduction

During the last decades, piezoelectric polymers like poly(vinylidene fluoride) (P(VDF)) [1,2] and polyamide 11 (PA 11) [3–6] have been very attracted since they can be associated with versatile morphology and attractive mechanical properties of organic polymers. By using copolymer of vinylidene fluoride trifluoroethylene (P(VDF-TrFE)) [7] and P(VDF-TrFE-CFE) terpolymers [8], the experimental procedure to obtain piezoelectric phases have been considerably facilitated. Nevertheless, the poling procedures remain more difficult in regards to inorganic ferroelectric ceramics such as barium titanate (BT) [9]. An interesting approach to optimize piezoelectric properties has been to associate organic polymers with inorganic piezoelectric ceramics so as to elaborate hybrid composites with thermoplastic matrix [10,11] or elastomeric one [12]. Since suitable mechanical properties requires low volume fraction of inorganic particles, the next step has been to introduce sub micronic inorganic particles. For example, Chan et al. [13] have been obtained interesting engineering parameters using fluorinated polymers. In this work, sub micronic BT particles have been homogeneously dispersed in an engineering polyamide (PA 11) to elaborate 0–3 composite. The influence of BT volume fraction on longitudinal piezoelectric strain coefficient of such composites has been previously published [14]. In this manuscript, we will focus on the influence of the polarization procedure (time, temperature, and electric field) on the piezoelectric properties of the nanocomposites as a function of particles size and nanotexture. Structure/property relationships will be established using data from diathermal scanning calorimetry (DSC), thermally stimulated current (TSC), X-ray diffraction (XRD) and high-resolution transmission electron microscopy (HRTEM). Engineering properties will be discussed using the merit factor.

2. Experimental

2.1. Materials and polarization procedure

[1]Polyamide 11 has been studied in its unpoled state. The mean diameter of [2]$BaTiO_3$ was 700, 300, 100 and 50 nm, respectively. PA 11 powder was dissolved in a solution of dimethyl acetyl amide (DMAc) at 160 °C and the required $BaTiO_3$ was dispersed by ultrasonic stirring in order to form a mixture. The samples were dried

* Corresponding author.
E-mail address: dantras@cict.fr (E. Dantras).

[1] PA 11 was supplied by Arkema (France).
[2] $BaTiO_3$ by Inframat materials (USA).

over night at 110 °C to remove the traces of solvent. The nanocomposites were hot pressed to form thin films from 70 to 100 μm thickness. Volumic ratio was determined by density measurements from a mixture law: $d_{composite} = (1 - \phi)\ d_{PA11} + \phi\ d_{BT}$ (with $d_{PA11} = 1.05$, $d_{BT} = 6.05$ and ϕ the volumic ratio). The volumic ratios (ϕ) of nanoceramic in composite films were 0.1, 0.2, and 0.4, respectively. For electric polarization, gold electrodes were evaporated on both sides of thin films by cathode pulverization. Nanocomposites were poled to orient the electrical dipoles of nanometric ceramics; a macroscopic polarization P was obtained. The films were polarized in an oil bath to prevent any voltage breakdown. The heating of the oil bath was performed with an accuracy of 3 °C. Electric signal was generated by a ±10 V generator and then amplified using a ×2000 voltage amplifier. The electric field E was progressively increased until the required voltage and kept constant 30 min. It was removed before short-circuit. To check the poling process, the current versus the applied field was measured (for purpose of clarity these data will not be reported). The samples were short-circuited to relax the internal stress induced during the poling and then annealed at room temperature for 1 day. The value of coercitive field for $BaTiO_3$ and PA 11 were determined near 3 and 100 kV/mm, respectively.

2.2. Methods

2.2.1. Scanning electron microscopy

JEOL JSM 6700F-scanning electron microscope with field emission gun (SEM-FEG) was used to study BT dispersion in the polyamide matrix. As BT density is higher than polyamide one, backscattered electron detection was used. The dispersion of 700 nm BT particles has been analyzed by FEG-SEM microscopy. Fig. 1(a,b) (at different magnification) shows a homogeneous dispersion of particles (white contrast) in the PA matrix for a high filler content ($\phi = 0.4$). This dispersion is free from agglomeration even for the large scale. The BT particles are separately included in the polymer matrix.

2.2.2. Standard diathermal scanning calorimetry

Standard diathermal scanning calorimetry (DSC) measurements were performed using a DSC/TMDSC 2920 set up. The sample temperature and the heat-flow were calibrated using standard procedure. The glass transition temperature of PA 11 was determined near $T_g = 45$ °C. The ferroelectric to paraelectric phase transition of the particles (endothermic peak) were measured by standard DSC using a heating scan q_h of +10 °C min^{-1}. DSC measurements were performed on BT nanopowders (Fig. 2). The Curie transition of BT is characterized by an endothermic peak near 130 °C. Fig. 2 shows a small decrease of the enthalpy of ferro/paraelectric phase transition for the particles of 300 nm compared with 700 nm particles. This fact corresponds to a decrease of the Curie temperature (T_c) probably due to a size effect observed in the following experimental section. We do not point out any phase transition for the 50 and 100 nm particles by DSC.

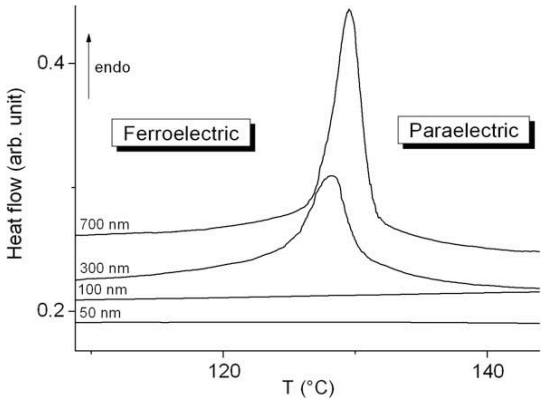

Fig. 2. Curie transition of BT nanoparticles for various nanosize obtained by DSC.

2.2.3. Dynamic dielectric spectroscopy

A novocontrol broadband dielectric spectrometer system BDS 400 was used to obtain the dielectric permittivity. Isothermal measurements were carried out. The complex dielectric permittivity $\varepsilon^*(\omega,T)$ was recorded. The real part of the dielectric permittivity, ε', used to do calculation, was extracted from the isotherm 25 °C and for the frequency 1 kHz ($BaTiO_3$ monocrystal $\varepsilon' = 1500$). Real part of the dielectric permittivity change across the dynamic glass transition of PA 11 is equal to $\Delta\varepsilon = 5.5 \pm 0.2$ at $T_\alpha = 50$ °C.

2.2.4. Piezoelectric measurements

Piezoelectric measurements were carried out using a PM 200 piezometer supplied by Piezotest (UK), with a force of 0.25 N at 110 Hz in frequency. The piezoelectric coefficient d_{33} (pC/N) is measured in the same direction than the polarization field, following the relation:

$$P = d_{33} \times \sigma$$

where P is the polarization (C/m^2) and σ the applied stress (N/m^2). As example, the d_{33} value of $BaTiO_3$ monocrystal is around 90–100 pC/N at 25 °C.

2.2.5. Thermally stimulated current

Complex TSC thermograms were carried out on a TSC/RMA Analyser. For complex experiments, the sample was polarized by an

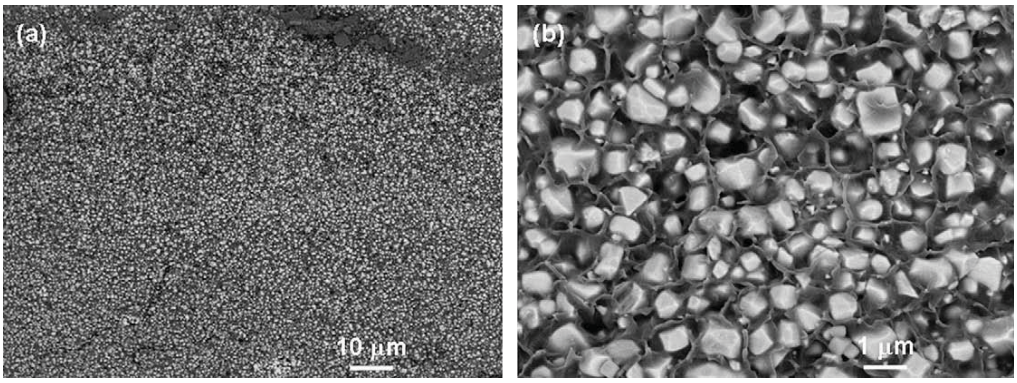

Fig. 1. FEG-SEM images of PA 11/BT nanocomposites for ϕ 0.4 and 700 nm in diameter (a) ×1000 and (b) ×10,000.

electrostatic field $E_p = 1$ MV m^{-1} during $t_p = 2$ min over a temperature range from the polarization temperature $T_p = 80$ °C down to the freezing temperature $T_0 = 0$ °C. Then the field was turned off and the depolarization current was recorded with a constant heating rate ($q_h = +7$ °C min^{-1}), the equivalent frequency of the TSC spectrum was $f_{eq} \sim 10^{-2}$–10^{-3} Hz.

2.2.6. X-ray diffraction

The diffraction pattern of $BaTiO_3$ powder were measured using a Powder diffractometer (D8) with carbon-filtered Cu Kα (1.54056 Å) source. Powder XRD pattern were taken in the continuous mode, over a range of 44–46.5° 2θ with 0.01 degree step size and 5 s dwell per step.

2.2.7. $BaTiO_3$ nanoparticles microstructure

To precisely determine the structure/texture of the $BaTiO_3$ nanoparticles, investigations were made using high-resolution transmission electron microscope (HRTEM). A drop of the different $BaTiO_3$ nanoparticles suspension was put on commercially copper grids coated with lacey carbon films. Electron transparent samples were obtained. The TEM and HRTEM imaging were performed using a FEI Tecnai F20 S-TWIN microscope. The elemental composition was also deduced by Energy Dispersive Spectroscopy (EDS) at nanometer scale. The diffraction patterns were obtained using the selected area diffraction (SAED) of by Fourier transform of the HRTEM images.

3. Results and discussion

3.1. Dependence of the piezoelectric behaviour of the nanocomposite on polarization conditions

The longitudinal piezoelectric strain coefficients d_{33} of PA 11/$BaTiO_3$ 700 nm composite with volume fraction of BT ranging from $\phi = 0.1$ to 0.4 were investigated. Fig. 3(a) shows the evolution of the piezoelectric coefficient of a PA 11/$BaTiO_3$ composite as a function of the polarization time. The polarization of the samples was performed at $T_{pol} = 40$ °C. This temperature T_{pol} has been chosen in the vicinity of the PA 11 glass transition temperature. This point will be discussed later. The poling field was 3.3 kV/mm. Error bars, obtained for different samples poled at the same time, have been added on each value of piezoelectric coefficient. We note a good stability of piezoelectric coefficient even at high volume fraction of BT. A plateau of the piezoelectric coefficient is reached above 16 min of polarization. The order of magnitude of this time constant suggests that the establishment of the local field might be governed by macromolecular mobility and interfacial polarization.

Fig. 3(b) illustrates the evolution of the piezoelectric coefficient as a function of the polarization temperature. Samples were heated up to the required temperature in an oil bath and then polarized under a field of 3.3 kV/mm for 30 min. Then, samples were cooled to room temperature under electrostatic field. When they have reached the room temperature, the field was removed and the samples were short-circuited for 5 min. Fig. 3(b) points out a threshold of the piezoelectric coefficient near 50 °C. We report also on this Figure, the depolarization current obtained by TSC as a function of temperature. The primary mode of PA 11 situated at $T_\alpha = 55$ °C is extracted. TSC measurements allow us to determine the α mode associated with the dielectric manifestation of the PA 11 glass transition [14]. This mode appears in the same temperature range as piezoelectric coefficient threshold. The threshold of the piezoelectric coefficient of the composites shown on Fig. 3(a) is explained by the fact that the BT particles are dispersed in the amorphous phase of polyamide 11. Around the glass transition temperature, molecular mobility involved in the polymeric matrix

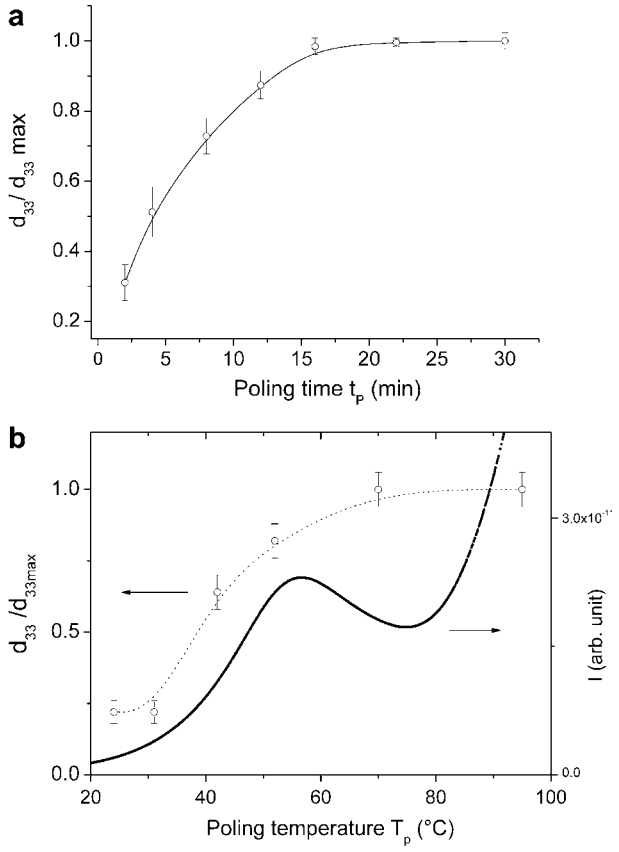

Fig. 3. (a) Normalized piezoelectric coefficient versus polarization time of PA 11/BT 700 nm composite with $\phi = 0.4$ (the value of d_{33max} is extracted from Fig. 6) and (b) normalized piezoelectric coefficient versus polarization temperature of PA 11/BT 700 nm composite with $\phi = 0.4$ (the value of d_{33max} is extracted from Fig. 6) and TSC depolarization current of PA 11 matrix.

increases allowing the establishment of the local field. The polarization of the BT particles increases the piezoelectric coefficient from 1 pC/N below T_g to 5 pC/N above T_g. This last value is higher than for poled PA 11 value [3].

The dependence of d_{33} with the applied field is reported on Fig. 4. The field was applied on each sample for 30 min at 90 °C.

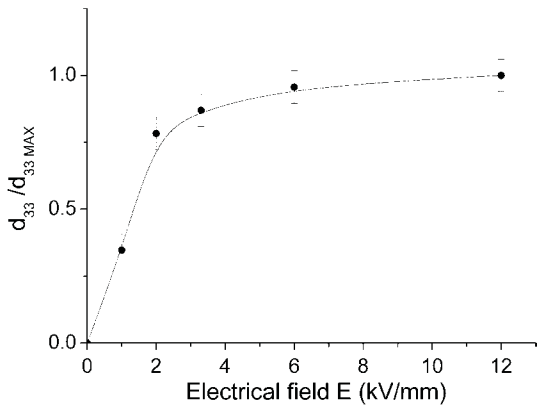

Fig. 4. Influence of the applied field on the normalized piezoelectric coefficient of a PA 11/BT 700 nm composite with $\phi = 0.2$ (the value of d_{33max} is extracted from Fig. 6).

Samples were cooled under field. The field was switched off and samples were short-circuited during 5 min. This Figure pointed out that the d_{33} reaches a plateau for an applied field value superior to 3.3 kV/mm. It is important to note that an analogous value is recorded for the inorganic BT ceramic. This result shows that, in those conditions, the local field is comparable with the external electric field [10].

3.2. Dependence of the nanocomposite piezoelectric behaviour on particles size

Fig. 5 shows the influence of particles size on the polarization time. The experiments were performed in the same experimental conditions as previous part. No major influence of the particles size on the polarization time has been pointed out. The polarization time of composite is not size dependant.

Fig. 6 reports the influence of the piezoelectric coefficient with the volume fraction of BT for different particles size. This figure exhibits a linear increase of the piezoelectric activity of the composite independently of the particles size. For a constant volume fraction, we observe a low decrease of d_{33} for the composite made with 700 and 300 nm BT particles and an important one for the composite with 100 nm particles. Composites with 50 nm particles are not piezoelectric. The decrease of the piezoelectric activity of the composite with the nanofiller size reported on Fig. 6 is mainly due to the evolution of the tetragonal phase of particles. It has been followed by diathermal scanning calorimetry on Fig. 2. The enthalpy of the Curie transition was measured as a function of particles size and we observe a slightly decrease of ΔH_{curie} between 700 and 300 nm from 0.7 to 0.5 J/g. Ferroelectric/paraelectric transition was not observed for 50 and 100 nm particles. This fact is in agreement with data reported by several authors [15–17]. The DSC technique permits to follow the Curie transition of BT particles until 100 nm. Yan et al. reports by XRD measurements performed on BT particles that a tetragonal phase is still present for 100 nm BT particles [18]. This fact explains the piezoelectric activity reported for the PA/BT 100 nm nanocomposite. In order to precisely determine the structure and the nanotexture, BT particles were studied by XRD and TEM. XRD analysis of all BT particles leads to the diffractograms reported on Fig. 7 over a range of 2θ from 44 to 46.5°. The 50 and 100 nm BT particles presents only one Bragg peak located around 45.2°, which corresponds to the (2 0 0) plane of the cubic phase (PCPDF file 79-2263). For the 300 and 700 nm $BaTiO_3$ particles, two Bragg peaks located around 44.8 and 45.4° are present and correspond to the (0 0 2) and (2 0 0) planes of the tetragonal phase (PCPDF file 81-2203), respectively. So the 50–100 nm BT are cubic while the others are tetragonal. The lattice parameters *a* and *c* from all BT particles have been obtained from the diffraction data and are shown in Table 1. A slight long-range tetragonal lattice distortion starts to appear in BT samples at 300 nm. The cubic/tetragonal transition seems to take place between the particle size of 100 and 300 nm.

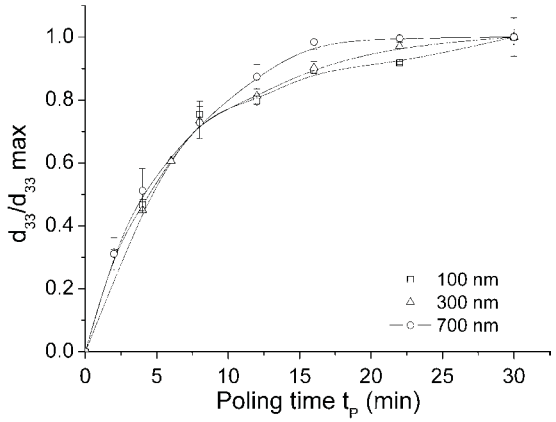

Fig. 5. Normalized piezoelectric stain coefficient versus polarization time of PA 11/BT composite with $\phi = 0.4$ for various nanosized particles (the value of d_{33max} is extracted from Fig. 6 and $T_{poling} \sim 70$ °C).

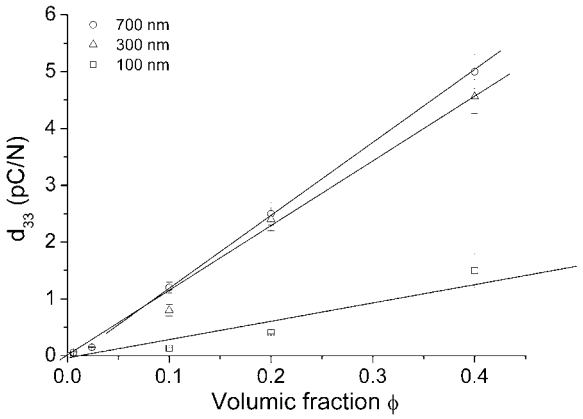

Fig. 6. Piezoelectric strain coefficient versus BT volume fraction ϕ for various nanosize particles ($T_{poling} \sim 70$ °C).

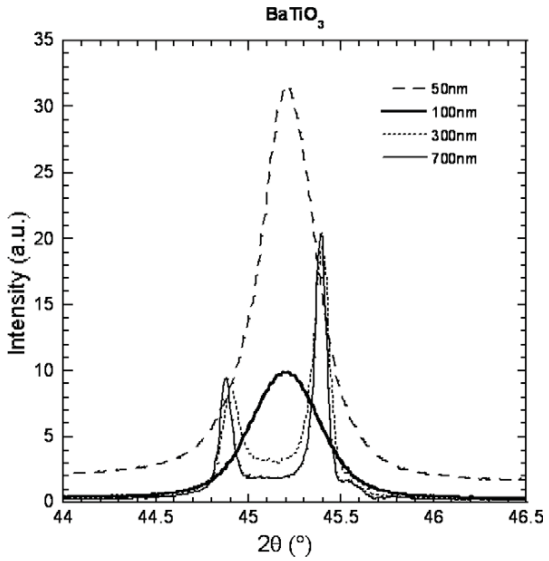

Fig. 7. X-ray diffraction analysis on the $BaTiO_3$ powders as a function of particles size.

Table 1
Particles size and lattice parameters of $BaTiO_3$ particles.

Specimen	a (Å)	c (Å)	c/a (ratio)
$BaTiO_3$ – cubic PCPDF-79-2263	4.006(2)		1
$BaTiO_3$ – 50 nm	4.008(2)		1
$BaTiO_3$ – 100 nm	4.008(6)		1
$BaTiO_3$ – 300 nm	3.9917(2)	4.033(5)	1.0104
$BaTiO_3$ – 700 nm	3.9931(4)	4.036(4)	1.0108
$BaTiO_3$ – tetragonal PCPDF-81-2203	3.99095(29)	4.0352	1.0111

So as to precisely determine the cubic/tetragonal transition, the nanotexture of these particles has been investigated by TEM and HRTEM. The study concerning the 50 and 100 nm BT is represented on Fig. 8(a,b) and (c,d), respectively. The bright-field TEM image of 50 nm BT (Fig. 8(a)) shows a constant distribution of particle size around 50 nm and a homogeneous spherical morphology. The high-resolution image (Fig. 8(b)) of one BT particle is characteristic of a well-crystallized crystal (monolith). Moreover, by the way of the Fourier transform of HRTEM image, we can determine that the 50 nm BT is only composed of cubic phase at a nanometer scale. On the other hand, for the 100 nm BT, Fig. 8(c) exhibits also a homogeneous morphology of particles but the high-resolution study shows that the core of the particle is composed of the tetragonal phase whereas the shell is constituted of cubic structure. The Fourier transform of the different part of the particle correspond to the presence of cubic BT at the edge and tetragonal BT inside the particle. Moreover, between this two phases, we have an intermediate phase (schematized around the white line – 2–3 nm size) where the composition is between the cubic and the tetragonal phase. This fact has been determined by Fourier transform. This investigation permits to determine that the cubic/tetragonal transition has taken place between 50 and 100 nm particle sizes in good agreement with the study of Yan et al. [18]. So a model can be extrapolated due to the TEM results. This model represented on Fig. 9 shows that the core of a 100 nm BT is tetragonal where as the shell is cubic with the presence of a tetragonal gradient between the extreme parts.

These HRTEM observations confirm previous data obtained using a synchrotron radiation X-ray diffraction. Hoshina et al. [19] find that the $BaTiO_3$ nanoparticles have composite structures consisted of an internal tetragonal layer, a Gradient-Lattice-Strain Layer (GLSL) and a surface cubic layer. The intermediate phase is also pointed out in this study and the complex internal nanotexture is shown by HRTEM. Furthermore, these authors suggest that the ferroelectric critical size of $BaTiO_3$ is about 20–30 nm. We do not observed a ferroelectric phase for 50 nm particles, we suggest that the cubic/tetragonal transition is between 50 and 100 nm. For the specific case of 100 nm particles, a substantial reduction of the effective volume of ferroelectric phase could explain the smearing out of the transition; thermal analysis is not able to discriminate the endothermic peak associated with the enthalpy of ferro/paraelectric phase transition.

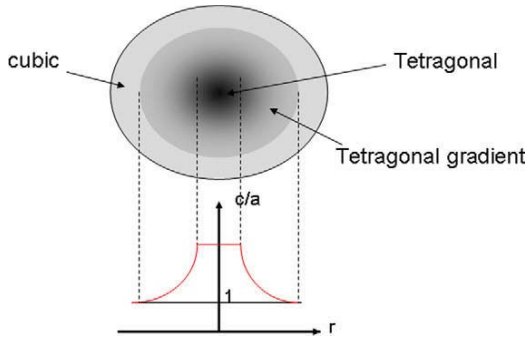

Fig. 9. Core–shell structure of 100 nm BT particles, ratio between tetragonal and cubic phase is illustrative only.

Furthermore, the small shift of T_c ($\Delta T_c = 1.4\,^{\circ}C$) between 700 and 300 nm shown on Fig. 2 can be also explained by the core–shell phenomenon. On the basis of a thermodynamic model, the small shift of T_c with size particles has been already predicted and observed [20] but for size below 200 nm. Due to core–shell microstructure, the real tetragonal phase diameter is well below 300 nm, closer to 200 nm.

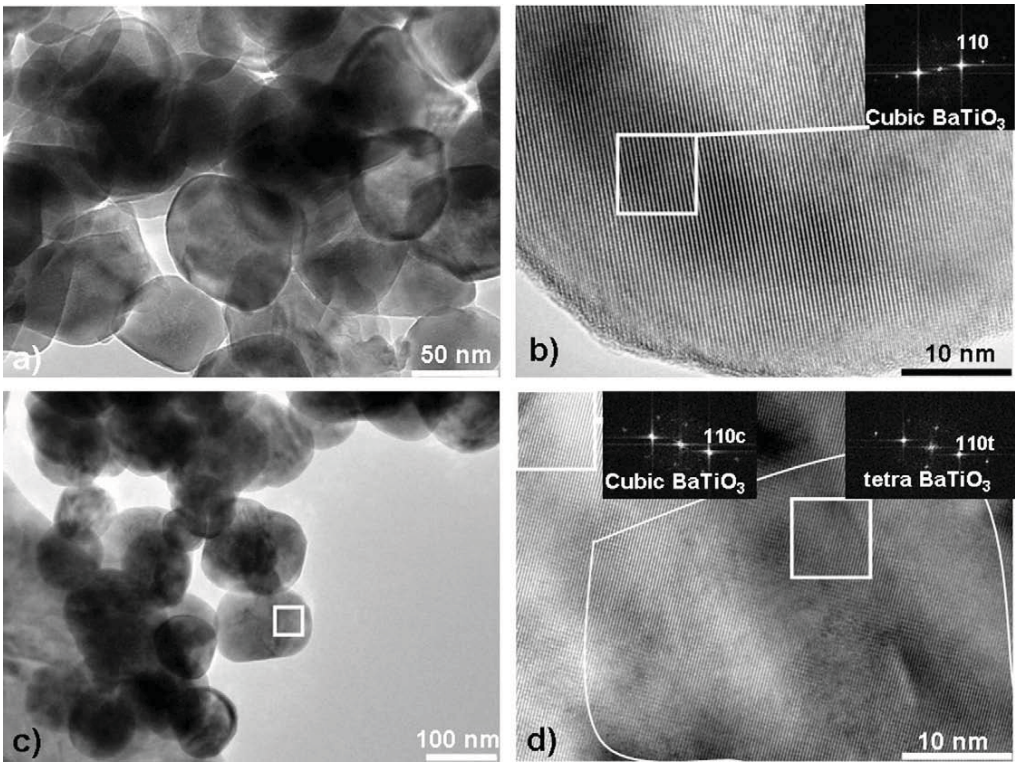

Fig. 8. (a) Bright-field TEM (b) HRTEM images of 50 nm BT particle (c) BF TEM and (d) HRTEM images of 100 nm BT particle.

3.3. Dependence of the nanocomposite piezoelectric voltage coefficient on volume fraction

The piezoelectric voltage coefficient is defined by:

$$g_{33} = d_{33}/\epsilon\epsilon_0$$

where ε is the dielectric permittivity of the nanocomposite and ε_0 is the dielectric permittivity of vacuum.

On Fig. 10, the real part of the dielectric permittivity of the PA 11/$BaTiO_3$ composites was measured by dielectric spectroscopy, is reported versus the volume fraction of inclusions. We note that the permittivity of the composite increases with BT volumic fraction range of 0.1–0.4, independently of particles size. This evolution is well fitted by the Bruggeman model [21] (solid line on Fig. 11, with $\epsilon'_{PA11} \sim 2.5$ and $\epsilon'_{BaTiO_3} \sim 1500$). FEG-SEM images (Fig. 1) confirms the existence of a homogeneous dispersion at a nanometric scale even at high volume fraction (composite with $\phi = 0.4$ volume fraction of 700 nm BT). The piezoelectric voltage coefficient g_{33} of PA/BT composite versus the volume fraction of BT is reported on Fig. 11. g_{33} reaches a maximum value only for $\phi = 0.2$ of BT. Note that the reduction of g_{33} with particles size is due to the decrease of the piezoelectric activity since the dielectric permittivity is independent of this parameter. We observe on Fig. 11 that the piezoelectric voltage coefficient g_{33} reaches a plateau only for $\phi = 0.2$. The g_{33} value decreases with particles size.

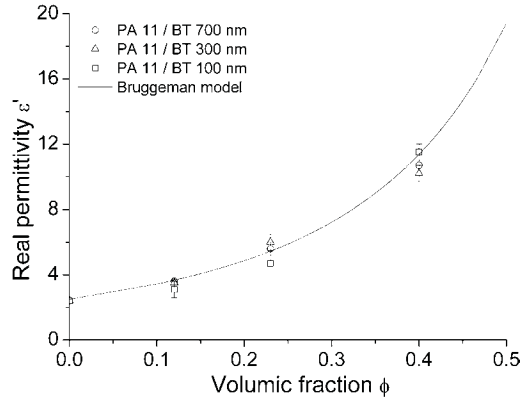

Fig. 10. Real part of the dielectric permittivity versus volume fraction ϕ of BT for composites with various nanosize particles, Bruggeman fit is in solid line.

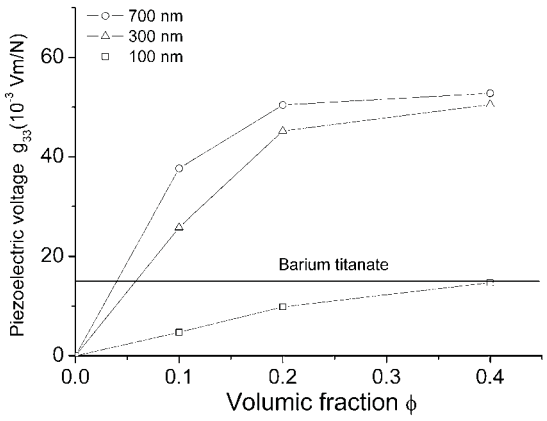

Fig. 11. Piezoelectric voltage coefficient versus BT volume fraction for composites with various nanosize particles, g_{33} value of $BaTiO_3$ bulk is reported in bold line.

Moreover, the maximum value of this parameter is higher than the piezoelectric voltage coefficient of BT. For PA 11/$BaTiO_3$ 700 nm composite, the g_{33} value is reached for less than 10% volume fraction of inclusion. The piezoelectric voltage coefficient of $BaTiO_3$ bulk reported on Fig. 11, has been calculated from d_{33} and ε' experimental value. Ceramics have higher piezoelectric coefficient than composite, but composite have much lower permittivity.

4. Conclusion

PA 11/$BaTiO_3$ nanocomposites with various particles sizes and volume fraction were elaborated. Poling conditions have been determined in order to elaborate poled ceramic/unpoled polymer composites. We found that the piezoelectric coefficient is highly poling temperature and time dependent. By poling the samples above the glass transition of the matrix, the maximum piezoelectric coefficient of the composite was reached in 16 min. The magnitude of the poling field (3.3 kV/mm) is analogous with the one used for BT i.e. significantly lower than for piezoelectric polymers (100 kV/mm). The optimum piezoelectricity is 5 pC/N for a PA 11/$BaTiO_3$ 700 nm with $\phi = 0.4$; it is reached when the amorphous phase of the polymeric matrix is in the liquid state i.e. for a polarization temperature higher the glass transition and for time constant allowing macromolecular mobility. Then, the local field becomes equivalent to the external field. The piezoelectric activity of composite decreases for BT particles lower than 300 nm due to the loss of tetragonal phase. An increase of the longitudinal piezoelectric strain coefficient d_{33} for increasing volume fraction of BT was shown. Contrary to inorganic piezoelectric ceramics, the dielectric permittivity of hybrid composites remains moderate although the piezoelectric voltage coefficient of composites is bigger. Due to the higher value of g_{33} of the composite compare to the ceramic value, these nanocomposites have potential applications as sensors. Finally, we shed some light on $BaTiO_3$ particles complex nanotexture and propose a ferroelectric critical size slightly above 50 nm.

Acknowledgements

The authors acknowledge the financial support from DGCIS and Région Midi-Pyrénées of NACOMAT.

References

[1] P.T.A. Klaase, J. van Turnhout, Third international conference on dielectric materials, Measurements and Applications IEE (1979) 411–414.
[2] G. Teyssedre, C. Lacabanne, Thermochim. Acta 226 (1993) 65–75.
[3] S.C. Mathur, J.I. Scheinbeim, B.A.J. Newman, Appl. Phys. 56 (1984) 2419–2425.
[4] S. Ikeda, T. Saito, M. Nonomura, T. Koda, Ferroelectrics 171 (1995) 329–337.
[5] L. Ibos, C. Maraval, A. Bernès, G. Teyssèdre, C. Lacabanne, S.-L. Wu, J.I.J. Scheinbeim, Polym. Sci. B 37 (1999) 715–723.
[6] L. Ibos, A. Bernes, C. Lacabanne, Ferroelectrics 320 (2005) 483–489.
[7] G.A. Samara, F. Bauer, Ferroelectrics 135 (1992) 385–399.
[8] Baojin Chu, Zhou Xin, B. Neese, Q.M. Zhang, F. Bauer, Ferroelectrics 331 (2006) 35–42.
[9] T.A. Perls, T.J. Diesel, W.I.J. Dobrov, Appl. Phys. 29 (1958) 1297–1302.
[10] T. Furukawa, K. Ishida, E.J. Fukada, Appl. Phys. 50 (1979) 4904–4912.
[11] K.H. Lam, H.L.W. Chan, Comput. Sci. Tech. 65 (2005) 1107–1111.
[12] D. Khastgir, K. Adachi, J. Polym. Sci., Part B 37 (1999) 3065–3070.
[13] H.L.W. Chan, S.T. Lau, K.W. Kwok, Q.Q. Zhang, Q.F. Zhou, C.L. Choy, Sens. Actuators, A 75 (1999) 252–256.
[14] J.-F. Capsal, E. Dantras, J. Dandurand, C. Lacabanne, J. Non-Cryst. Solids 353 (2007) 4437–4442.
[15] S. Wada, T. Hoshina, H. Yasuno, M. Ohishi, H. Kakemoto, T. Tsurumi, M. Yashima, Ceram. Eng. Sci. Proc. 26 (2005) 89–100.
[16] K. Suzuki, K. Kijima, J. Alloy. Compd. 419 (2006) 234–242.
[17] F. Baeten, B. Derks, W. Coppens, E. van Kleef, J. Eur. Ceram. Soc. 26 (2006) 589–592.
[18] T. Yan, Z. Shen, W. Zhang, J. Chen, Mater. Chem. Phys. 98 (2006) 450–455.
[19] T. Hoshina, S. Wada, Y. Kuroiwa, H. Kakemoto, T. Tsurumi, Sixteenth IEEE International Symposium on the Applications of Ferroelectrics 1 (2007) 476–477.
[20] Q. Jiang, X.F. Cui, M. Zhao, Appl. Phys. A 78 (2004) 703–704.
[21] D.A.G. Bruggeman, Ann. Phys. Lpz. 24 (1935) 635–679.